



Phase and size separations occurring during the injection of model pastes composed of β -tricalcium phosphate powder, glass beads and aqueous solutions



S. Tadier^{a,1}, L. Galea^a, B. Charbonnier^a, G. Baroud^b, M. Bohner^{a,*}

^aRMS Foundation, Bischmattstrasse 12, 2544 Bettlach, Switzerland

^bLaboratoire de Biomécanique, Département de Génie, Université de Sherbrooke, Sherbrooke, Québec J1K 2R1, Canada

ARTICLE INFO

Article history:

Received 31 October 2013

Received in revised form 2 December 2013

Accepted 10 December 2013

Available online 18 December 2013

Keywords:

Injectability

Filter-pressing

Liquid phase migration

Size separation

Calcium phosphate cement

ABSTRACT

Glass beads a few hundred micrometers in size were added to aqueous β -tricalcium phosphate pastes to simulate the effect of porogens and drug-loaded microspheres on the injectability of calcium phosphate cements and putties. The composition of the pastes was monitored during the injection process to assess the effect of glass bead content, glass bead size and paste composition on the paste injectability. The results revealed that the injection process led to both liquid and glass bead segregations: the liquid flowed faster than the glass beads, which themselves flowed faster than the β -tricalcium phosphate microparticles. In fact, even the particle size distribution of the glass beads was modified during injection. These results reveal that a good design of multiphasic injectable pastes is essential to prevent phase separation.

© 2013 Acta Materialia Inc. Published by Elsevier Ltd. All rights reserved.

1. Introduction

The discovery of calcium phosphate cement (CPC) in the early 1980s [1,2] has paved the way towards the design of biomaterials able to be implanted using mini-invasive surgery techniques, to fill perfectly all types of bone defects, regardless of their shape, and to set in situ to provide early mechanical properties. CPCs have therefore been extensively studied in the last 30 years [3,4].

One of the CPC drawbacks is their limited capacity to be extruded through a syringe coupled with a thin long cannula or, in other words, their poor injectability [5–7]. Indeed, upon extrusion of a mineral paste, a phase separation generally occurs between liquid and solid: the extruded paste contains more liquid than the initial one; thus, the paste remaining in the injection device gradually becomes water-depleted and a dense cake of particles forms at the plunger side [5,6,8]. This leads to non-homogeneity of the extrudate, deviation from the initial liquid to powder ratio, alteration of the in situ setting reaction and of the cement properties, and halting of the injection due to syringe plugging [3,5,6,8].

This phenomenon, also known and studied in some non-medical applications (soil mechanics, food industry, granulate and cementitious materials, extrusion/spherization processes, injection moulding of ceramics) [9–14] has been referred to as phase separation, phase migration or “filter-pressing” [5].

This phase separation mechanism has been detailed in previous studies, both from a theoretical [5,11,12] and from an experimental [5–9,11] point of view. Strategies are known to reduce or even eliminate filter-pressing: the predisposition of the liquid phase to filter through the solid phase has to be reduced. For example, both the use of finer or milled particles to fill the voids and decrease the permeability of the powder constituting the solid phase [5,8,15] and the addition of a hydrogel in the liquid phase to increase its viscosity [5,16] have been tested with success.

So far, these strategies have been applied to CPCs composed of a micro-sized powder (mean size typically close to 1–10 μm) and of a liquid. However, there has been a trend lately to incorporate larger particles in the cement paste [3,4,17–26], for example to create macroporosity and increase the rate of new bone formation [18,21,23,25], to release drugs and bioactive molecules [19,20,24], or even to release cells for tissue engineering and bone regeneration [17].

In parallel, another approach has also been proposed and studied in recent papers: designing injectable pastes consisting of calcium phosphate (CaP) granules conveyed by means of a hydrogel [22,27–31]. In this strategy, the inter-granular space and the ease

* Corresponding author. Tel.: +41 32 6441413; fax: +41 32 6441176.

E-mail address: marc.bohner@rms-foundation.ch (M. Bohner).

¹ Current address: Université de Lyon, INSA-Lyon, MATEIS, CNRS UMR 5510, 7 Avenue Jean Capelle, 69621 Villeurbanne Cedex, France.

of access to the surface of the granules permit the facilitation of cell invasion and the release of bioactive molecules.

In both these approaches (introduction of bigger particles in cement pastes and delivery of CaP granules), the use of millimeter-sized particles is likely to decrease the injectability of the pastes and increase the filter-pressing phenomenon. It also may lead to size separation. Indeed, previous studies have shown that finer particles in a bimodal suspension behave essentially as a fluid toward the coarser particles [32]. As CPC pastes are prone to phase separation between liquid and solid phases, the question arises whether it could also be liable to size segregation between coarser (100–500 μm) and smaller (1–10 μm) particles [33].

Therefore, the aim of this study is threefold: (i) to assess the effect of millisized particles on the injectability of a calcium phosphate paste and on the filter-pressing phenomenon occurring during the injection, (ii) to compare the injectabilities of cement pastes and of putties composed of large granules embedded in a hydrogel, and (iii) to investigate whether the extrusion of a paste loaded with beads leads to size separation between bigger and smaller particles. Aims (i) and (iii) were partly addressed in a previous extended abstract [34].

To allow deeper investigation of the injectability and of the filter-pressing phenomenon, a model system was selected: the pastes were composed of non-setting mixtures of β -tricalcium phosphate (β -TCP; β - $\text{Ca}_3(\text{PO}_4)_2$) powder, water or hydrogel solution and millimeter-sized spherical particles. The latter beads consisted of non-soluble glass beads (mean diameter ranging from 150 to 400 μm).

2. Materials and methods

2.1. Pastes and putties preparation

In this paper, the word “paste” designates a mixture made of β -TCP powder (P), glass beads (B) and a liquid phase (L), which models the typical cement pastes. The word “putty” designates the association of beads together with a hydrogel carrier (B + L), which does not contain any β -TCP powder.

In all the pastes, the model powder was β -TCP ($\text{Ca}_3(\text{PO}_4)_2$, purum p.a., art. No 21218, Sigma–Aldrich, Steinheim, Germany; density = 3.1 g cm^{-3}). Its particle size distribution was measured in demineralized water with a laser diffraction particle size analyzer (LS 13 320, Beckman-Coulter, Krefeld, Germany). Its morphology was observed using a scanning electron microscope (EVO MA25, Zeiss, Germany) and the following protocol: the powder was suspended in ethanol; a drop of this suspension was spread on a sample holder and after evaporation of the solvent, the powder was coated with platinum during 60 s. This corresponded to a Pt layer thickness of 10 nm. The β -TCP powder was chosen for two main reasons: it has similar properties compared to the CaP powders commonly used for bone cements (e.g. its particle size distribution) and it does not set when in contact with a liquid phase. It is thus possible to explore the filter-pressing phenomenon in a reproducible manner without time constraints or risk of rheological evolution of the paste during the time elapsed between injection tests and samples characterization.

The liquid phase of pastes consisted either in demineralized water or in 0.5 wt.% sodium hyaluronate solution, prepared by dissolving sodium hyaluronate (Na hyaluronate 2.0 MDa, Lifecore Biomedical) in demineralized water, and stirred overnight to ensure a complete dissolution of the powder and hydration of the polymer molecules. The latter Na hyaluronate solution was also used as the liquid phase for putties. It was assumed that its density was 1 g cm^{-3} .

Different weight percentages (0–42%) and sizes (diameters between 156 and 390 μm) of glass beads (Spherglass[®] CP01 ref. 2024, 1922, 1821, 1619, Potters Europe; density = 2.5 g cm^{-3}) were introduced into pastes and putties. The weight percentages were calculated considering that the paste (P + B + L) represented 100% of the weight. As the amount of beads both before being introduced into the pastes and after injectability tests was assessed by measuring the beads' weight (see Section 2.3), the quantity of beads present in the various pastes was expressed as weight percentages. For example, 25, 36.5 and 42 wt.% corresponded, respectively, to volume percentages of 20, 30 and 35 vol.% of beads in the pastes (P + B + L = 100%) (Table 1). Bulk density of beads was assessed for all sizes: 100 g of beads were introduced into a graduated cylinder and pressed with a flat-bottomed tube to read the volume occupied by the beads directly on the cylinder scale. This volume was then used to calculate the bulk density. Measurements were done in triplicate and results were expressed as mean \pm standard deviation. The glass beads used here were chosen for their sphericity, for their diameters close to the typical sizes of particles usually introduced in cement pastes, and for their chemical stability in the liquid phases.

Powder and beads were first introduced into a plastic beaker (weight $\pm 1 \times 10^{-4}$ g) and manually pre-mixed; then the liquid phase was added with a fixed liquid-to-powder ratio (L/P, i.e. ratio of L/P) of 0.45 ml g^{-1} and the mixture was stirred manually with a spatula until the paste became homogeneous. Putties were prepared in a similar way: the glass beads were added to the sodium hyaluronate gel and mixed until an optically homogenous paste was obtained.

2.2. Injection tests

The injection test protocol was exactly the same for pastes and putties. After manual mixing of the components (P + B + L), the resulting paste was transferred into a 1 ml syringe (BD Luerlock, Beckton Dickinson, USA; inner diameter: 4.5 mm; opening diameter: 1.9 mm). This syringe type was used because similar syringes are used for bone augmentation procedures and because the syringe tip has a diameter in a typical range for cannulas used for cement injections. The plunger was then manually inserted from above into the vertically held syringe so that its lowest part reached the 1 ml graduation. In other words, a pre-load had to be applied onto the paste. The syringe was then inserted in a customized metallic gutter, which minimized the expansion of the syringe walls during the measurements (Fig. 1). The injection tests were performed without any cannula. Since the diameter of the biggest beads that were introduced into the pastes was 390 μm , the size ratio between the syringe opening diameter and the beads was close to 5.

Table 1

Conversion between vol.% and wt.% of glass beads within pastes and putties. B = beads, L = liquid phase, P = powder.

Pastes		Putties	
B/(L + P + B) (vol.%)	B/(L + P + B) (wt.%)	B/(L + B) (vol.%)	B/(L + B) (wt.%)
0	0	0	0
10	13	10	21.7
20	25	20	38.5
30	36.5	30	51.7
35	42	35	57.4
38.5	45.6	38.5	61
40	47	40	62.5
45	52.3	45	67.2
50	57.2	50	71.4
55	62	55	75.3

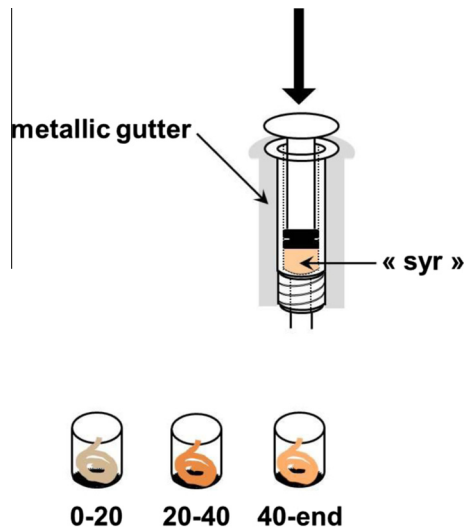


Fig. 1. Experimental set-up used for the injection tests. Three samples corresponding to different plunger displacement ranges were collected: in the first 20 mm of the plunger displacement (“0–20”), between 20 and 40 mm (“20–40”) and after 40 mm (“40–end”). The fourth sample was the paste remaining in the syringe (“syr”).

Injectability was measured using a compression testing machine (zwicki-Line Z5.0, Zwick, Kennesaw, GA, USA). The force applied on the plunger was recorded at a constant displacement rate of 0.4 mm s^{-1} . In this paper, the term “injectability curve” (load vs. plunger displacement) refers to the plot resulting from the average of at least three replicas (error bars representing standard deviations). The injection load was measured from the injectability curve: it was defined as the load at 5 mm of plunger displacement ($n > 3$) to avoid transient effects, as proposed by Bohner and Baroud [5].

Model pastes, which were extruded during these tests, were collected at three different displacement ranges, i.e. in the first 20 mm of the plunger displacement (hereafter denoted “0–20”), between 20 and 40 mm (“20–40”) and after 40 mm (from 40 to 60 mm when the paste was completely injectable, designated by “40–end”). Measurements were stopped when the load required to extrude the paste from the syringe reached 250 N.

The injectability of the paste was defined as the weight fraction of the paste which could be extruded from the syringe until a 250 N load was reached. When the paste was not fully injectable, the paste left in the syringe (“syr”) was then retrieved and analyzed together with the extruded samples. Hence, one tested paste led to a maximum of four samples after injection (“0–20”, “20–40”, “40–end” and “syr”; Fig. 1).

To evaluate the phase separation between liquid (L) and solid phase (P + B) during injection, two approaches were used. In the first approach, the slope of the intermediate region of injection curves was determined. In this paper, the value of this slope is mentioned as filter-pressing rate (or FP rate). In the second approach, the paste composition of the various samples collected during extrusion was followed.

2.3. Characterizations of samples after injection tests

Samples collected during injection tests were submitted to two successive processes. The first process involved a thermal treatment to either evaporate water (78 °C, 400 mbar, until constant weight was reached) or calcine the hydrogel solution (600 °C, 2 h). Tests performed on (P + B + L) blends of known composition showed that this protocol enabled the determination of the liquid

weight with a relative error smaller than 0.03%. The second process involved the dissolution of β -TCP powder in hydrochloric acid (HCl) solution. Briefly, after the removal of the liquid phase, the blends containing powder and beads were introduced into centrifugation tubes together with 7 ml of freshly prepared 1 M HCl (prepared from HCl 32%, Merck, Germany). Suspensions were first homogenized then centrifuged for 2 min at 4000 rpm (Centrifuge 5810R, Eppendorf, Hamburg, Germany). The HCl solution was refreshed and the process was repeated once to ensure a complete dissolution of the β -TCP powder. Then, the HCl solution was removed and replaced by 7 ml demineralized water to rinse the beads. The rinsing step was repeated, then water was poured out and the beads were dried in the drying oven with the same protocol as previously described (75 °C, 400 mbar). Tests performed on (P + B) standards showed that this protocol enabled the determination of the weight of beads within the blends with a relative error smaller than 0.03%. Moreover, when there were no beads in the tested pastes (reference pastes), the measurements led to a mean weight of $-0.0005 \pm 0.0004 \text{ g}$. They were all set to 0 for the calculations. The procedure described herein permitted the determination of the weights of L, P and B, thus allowing the calculation of $L/(P + B)$ and P/B ratios (wt.%) in the different portions of the extruded paste (“0–20”, “20–40” and “40–end”) and in the paste remaining in the syringe (“syr”).

Following these successive treatments, only the glass beads remained. Their sizes were determined by image analysis (Image Access 11 Premium, Imagic Bildverarbeitung AG, Glattbrugg, Switzerland) and compared to the size of as-received beads. To do so, the collected samples were shaken end-over-end for 1 min to ensure a homogeneous distribution. They were then dispersed on the surface of a white double-sided adhesive tape placed on a glass slide. The beads were examined using an optical microscope (Leica M250A). At least three pictures were taken on different locations on the slide and the diameter of all beads present on the photos was assessed. Measurements from the different micrographs were compared by statistical analysis to ensure that the results were representative of the samples. The median diameter D_{50} , i.e. the median point along the cumulative size distribution (50% of the beads were smaller than this value), was determined, as well as D_{10} and D_{90} (10 and 90%, respectively, of the beads were smaller than these values).

2.4. Statistical analysis

Bead size was varied with a constant bead fraction of 42 wt.% while bead volume fraction was varied with bead sizes of 156 and 390 μm . The composition of the paste was compared at different injection fractions (“0–20”, “20–40”, “40–end” and “syr”). The influence of bead size, bead fraction and injection fraction on the composition of the pastes and the injection force was analyzed by ANOVA tests on at least three replicas. Significance of differences was set at $p < 0.01$, unless stated.

3. Results

3.1. Characterization of powder and beads constituting the solid phase

The β -TCP powder had a monomodal particle size distribution with a median value (D_{50} in number) of $1.8 \pm 0.4 \mu\text{m}$. As shown in Fig. 2e, few particles were agglomerated.

Micrographies of the glass beads are presented in Fig. 2. In general, the D_{10} , the D_{50} and the D_{90} which were measured, were smaller than those provided by the supplier (Table 2). Moreover, the size ratio between the two components of the solid phase (i.e. β -TCP powder and glass beads) varied between 44 and 156.

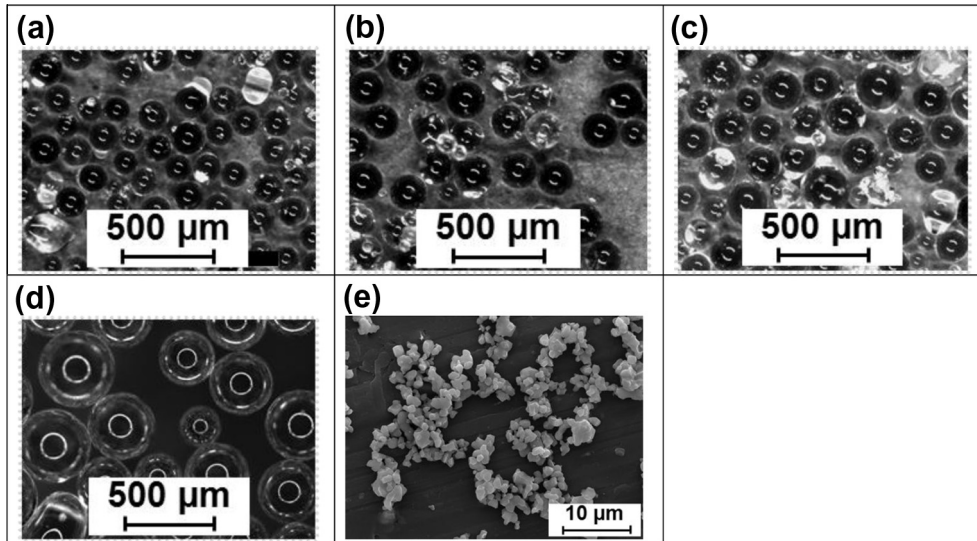


Fig. 2. Micrographs of the four different types of glass beads (B) and of the β -TCP powder (P): (a) 156 μm beads, (b) 203 μm beads, (c) 240 μm beads, (d) 390 μm beads, (e) β -TCP powder.

Table 2
SIZES OF THE GLASS BEADS: THE TWO FIRST COLUMNS CONTAIN VALUES PROVIDED BY THE SUPPLIER; THE THIRD AND FOURTH COLUMNS CONTAIN VALUES MEASURED IN THIS STUDY, AS DESCRIBED IN SECTION 2.3; THE FIFTH COLUMN CONTAINS THE D_{50}/D_{50} RATIO BETWEEN GLASS BEADS AND β -TCP POWDER (BOTH D_{50} VALUES MEASURED HERE); THE LAST COLUMN DISPLAYS THE BULK DENSITY OF THE BEADS.

D_{50} (μm) (supplier data)	D_{10} – D_{90} range (μm) (supplier data)	D_{50} (μm) (measured)	D_{10} – D_{90} range (μm) (measured)	Beads/ β -TCP powder size ratio (D_{50}/D_{50})	Bulk density (g cm^{-3})
156	106–212	80	16–157	44	1.429 ± 0.001
203	150–250	125	40–200	69	1.412 ± 0.006
240	180–300	120	34–212	67	1.437 ± 0.012
390	250–425	280	90–390	156	1.471 ± 0.002

For convenience, the D_{50} provided by the supplier was used to name the four different types of beads. For example, the smallest beads were denoted “156 μm beads”.

3.2. Injectability and injection force

To fulfill the goals of this study, it was necessary to extrude enough paste to be analyzed while simultaneously experiencing filter-pressing phenomena. Therefore, the test conditions were chosen so that the paste containing only β -TCP and demineralized water (0% beads) had an injectability slightly lower than 100% ($82 \pm 1\%$; Table 3): the plunger displacement reached 50 mm at the most (Fig. 3a), compared to 59 mm for empty syringes.

Injectability curves of the pastes were composed of three distinct zones (Fig. 3a). A very rapid increase of the load was observed during the first millimeters of displacement (Fig. 3b). In the second stage, the extrusion forces were characterized by a plateau in the absence of phase separation or by a slow increase when injectability was poor. In the last portion, the load increased

abruptly until 250 N, the load at which the injection system was stopped (Fig. 3a). Since the increase was so abrupt and the y-error bars became so large, it was decided to show only horizontal error bars. The horizontal error bars measured at 250 N correspond in fact to the error bars of the extruded weight shown in Fig. 2.

The percentage of extruded paste was significantly increased when a limited amount of 156 μm beads was introduced into the pastes (from $82 \pm 1\%$ without beads to $93 \pm 2\%$ with 42 wt.% beads; Table 3). Simultaneously, a tenfold increase of injection force was noticed (Table 3). With 390 μm beads, the injection force was also markedly increased (Table 3, Fig. 4), but the injectability either remained constant or dropped drastically (beyond 36.5% beads). Pastes made with 45.6% beads were not amenable to injection.

For pastes composed of a given bead volume and of demineralized water as liquid phase, Fig. 5 highlights that the total length of the plunger course was reduced with increasing size of included beads (data for 203 μm beads are not plotted for clarity reasons). More specifically, it decreased drastically when using beads of

Table 3
Injectability, injection load and filter-pressing (FP) rate of model pastes containing different sizes and amounts of beads ($n \geq 3$).

	Beads fraction (B) (wt.%)	0	13	25	36.5	42	45.6
156 μm beads	Injectability (%)	82 ± 1	n.t.	86 ± 8	n.t.	93 ± 2	87 ± 10
	Load at 5 mm (N)	1.5 ± 0.1	n.t.	3 ± 2	n.t.	14 ± 8	16 ± 8
	FP rate (N mm^{-1})	0.3 ± 0.2	n.t.	0.1 ± 0.1	n.t.	0.4 ± 0.2	0.7 ± 0.3
390 μm beads	Injectability (%)	82 ± 1	83 ± 4	79 ± 2	81 ± 5	35 ± 5	Not amenable to injection
	Load at 5 mm (N)	1.5 ± 0.1	3 ± 2	14 ± 9	23 ± 11	35 ± 16	Not measurable
	FP rate (N mm^{-1})	0.3 ± 0.2	0.4 ± 0.2	0.7 ± 0.2	2.7 ± 0.4	5 ± 1	Not measurable

Some mixtures were not tested (“n.t.”), so no values were reported. Beyond 42 wt.% of 390 μm beads, it was no longer possible to conduct injection experiments: the paste remained blocked in the syringe.

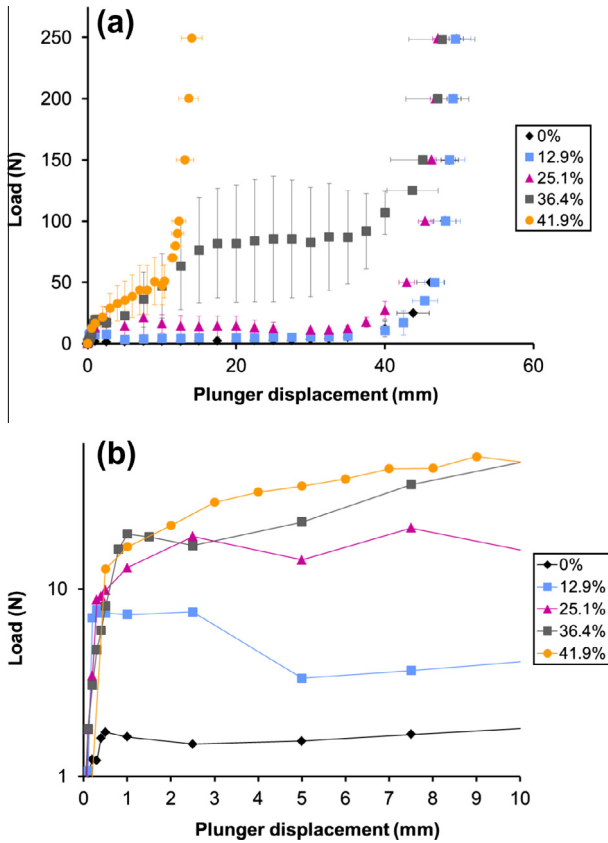


Fig. 3. (a) Injectability curves presenting the evolution of the extrusion force with the plunger displacement for pastes containing different percentages (wt.%) of 390 μm beads ($n \geq 3$ for each curve, error bars represent SD). (b) Zoom of the beginning of the injectability curves for pastes containing different percentages of 390 μm beads (error bars have been removed for clarity reasons).

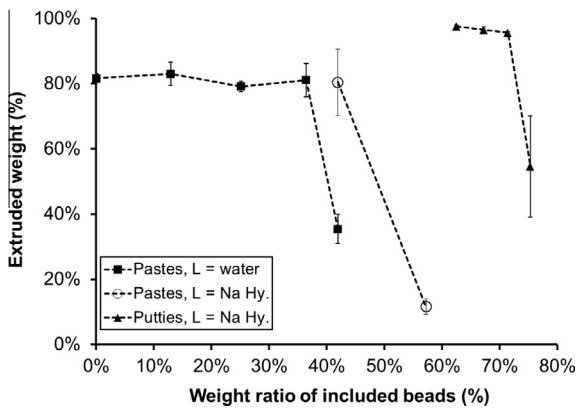


Fig. 4. Comparison of the injectability (= extruded weight) of model pastes prepared with different liquid phases (L = demineralized water and L = 0.5% Na hyaluronate solution) and of putties (L = 0.5% Na hyaluronate solution), as a function of the weight ratio of included 390 μm beads.

diameter 390 μm instead of 240 μm. Injectability also dropped with increasing bead size. For the 42 wt.% bead fraction, the percentage of extruded paste reduced from 93 ± 2% for the 156 μm beads to 35 ± 5% for the 390 μm ones. A concomitant increase in injection load was also noticed (Table 4).

Different routes have been proposed in the past to improve the injectability of mineral pastes; two of them were selected and investigated here. The first strategy was to increase the viscosity

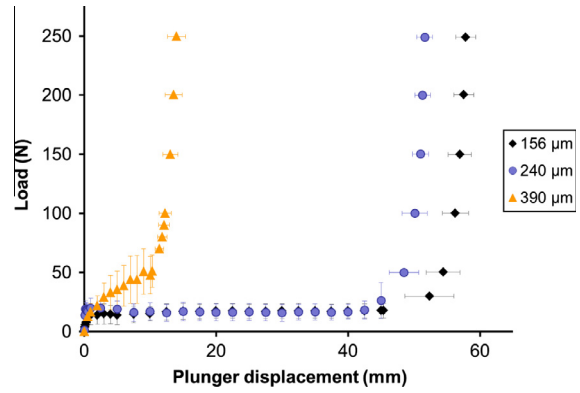


Fig. 5. Injectability curves presenting the evolution of the extrusion force with the plunger displacement for pastes containing 42 wt.% beads of different sizes ($n \geq 3$ for each curve, error bars represent SD).

Table 4

Injectability, injection load and filter-pressing rate of model pastes prepared with demineralized water or with 0.5% sodium hyaluronate solution (NaHy) (percentage of included beads = 42 wt.%) ($n \geq 3$).

Liquid phase	Demineralized water				0.5% NaHy
D_{50} of the beads (μm)	156	203	240	390	390
Injectability (%)	93 ± 2	90 ± 6	87 ± 3	35 ± 5	80 ± 10
Load at 5 mm (N)	14 ± 8	11 ± 6	19 ± 7	35 ± 16	5 ± 3
FP rate (N mm ⁻¹)	0.4 ± 0.2	0.4 ± 0.1	0.6 ± 0.5	5 ± 1	0.7 ± 0.6

of the liquid phase: a 0.5% sodium hyaluronate solution was used instead of demineralized water. For the same volume and size of included beads, this permitted both the increase in the injectability of the paste from 35 ± 5 to 80 ± 10% and the reduction of the injection load sevenfold (Fig. 4, Table 4): it dropped to 5 ± 3 N, which was a lower value than the load required to extrude pastes prepared with demineralized water, regardless of the size of included beads (Table 4). However, the 80 ± 10% injectability was still significantly lower than the extruded percentage when putties (same B and same L but no P) were used instead (Fig. 4). Moreover, a further increase of bead volume (from 42 to 57.2 wt.%) resulted in a very low injectability of 12 ± 2% (Fig. 4).

The second approach investigated here was the use of a broader bead size distribution. In this view, a mixture of the smallest and the biggest beads (156 μm and 390 μm) was prepared. The total amount of beads within the paste (i.e. $B/(L + P + B)$) was set to 42 wt.% but the proportion of the smallest beads compared to the biggest ones varied. Results are given in Table 5. Adding only 1/3 of 156 μm beads resulted in a better packing of the beads: the bulk density of the beads rose from $1.471 \pm 0.002 \text{ g cm}^{-3}$ for 390 μm beads only to $1.517 \pm 0.000 \text{ g cm}^{-3}$ for the blend (Table 5). A large increase of injectability was also experienced, from 35 ± 5 to 85 ± 5%, which was close to the injectability of the paste containing only 156 μm glass beads (93 ± 2%) (Table 5).

3.3. Phase separation

Two approaches were used to evaluate phase separation between liquid (L) and solid phase (P + B) during injection. In the first approach, the paste composition (L/(P + B) ratio) of the various samples collected during extrusion was monitored. In the second approach, the filter-pressing rates of the pastes (slopes of the

Table 5
Bulk density of bead blends and injectability, injection load and filter-pressing rate of model pastes containing a mixture of 156 μm and 390 μm beads (the total amount of beads was kept constant = 42 wt.%) ($n \geq 3$).

Fraction of 156 μm beads	1	2/3	1/2	1/3	0
Bulk density (g cm^{-3})	1.429 ± 0.001	1.494 ± 0.011	1.512 ± 0.006	1.517 ± 0.000	1.471 ± 0.002
Injectability (%)	93 ± 2	90 ± 3	86 ± 2	85 ± 5	35 ± 5
Load at 5 mm (N)	14 ± 8	10 ± 10	12 ± 3	21 ± 22	35 ± 16
FP rate (N mm^{-1})	0.4 ± 0.2	0.3 ± 0.3	0.3 ± 0.1	0.25 ± 0.06	5 ± 1

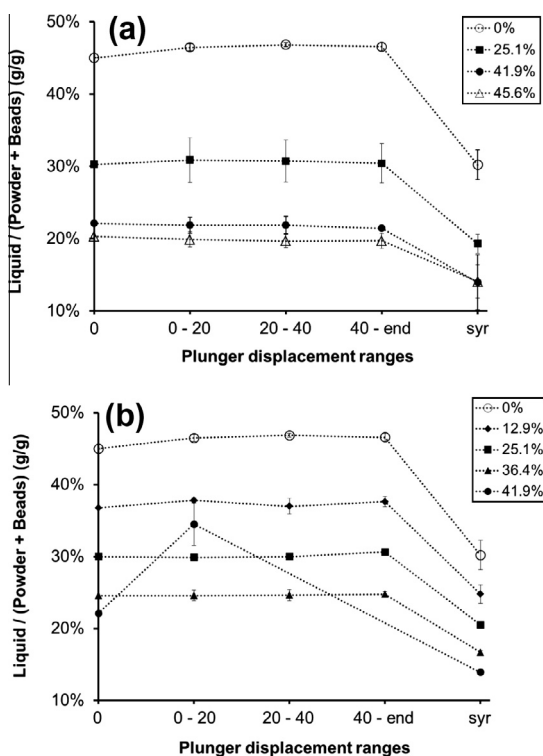


Fig. 6. (a) $L/(P+B)$ ratio in extruded samples and in the remaining paste (“syr”) as a function of the plunger displacement range (0–20, 20–40 and 40–end) for different weight fractions of 156 μm beads. The bars represent the standard deviation. (b) $L/(P+B)$ ratio in extruded samples and in the remaining paste (“syr”) as a function of the plunger displacement range (0–20, 20–40 and 40–end) for different weight fractions of 390 μm beads. The bars represent the standard deviation.

injection curves in the intermediary part) were determined and analyzed (Tables 3–5).

The $L/(P+B)$ ratio of the pastes remained constant throughout the injection (from 0 to end, Fig. 6). This “extruded $L/(P+B)$ ratio” was significantly higher than the initial $L/(P+B)$ ratio and higher than the $L/(P+B)$ ratio of the paste remaining in the syringe (“syr”, Fig. 6, Table 6). These results indicate that the extruded paste contained proportionally more liquid than the initial one. As a result, the paste remaining in the syringe was water-depleted and its final $L/(P+B)$ ratio was low. Interestingly, the final $L/(P+B)$

ratio (“syr”) varied with the amount of introduced beads but was independent of their sizes. For example, for 42 wt.% of included beads, the $L/(P+B)$ ratio of the paste remaining in the syringe was equal to 14 wt.% independently of the beads size (Table 6).

The filter-pressing rates were different for the smallest and the biggest beads. No matter how many 156 μm beads were added into the pastes, the FP rate remained unchanged (Table 3). On the contrary, with 42 wt.% 390 μm beads, the FP rate increased from $0.3 \pm 0.2 \text{ N mm}^{-1}$ without beads to $5 \pm 1 \text{ N mm}^{-1}$ (Table 3). In the latter case, the high FP value was related to liquid phase migration since the extruded $L/(P+B)$ ratio was $35 \pm 3\%$, i.e. more than 1.5 times the initial one (Table 6).

Examining the effect of the bead size at 42 wt.%, there was only a significant increase of the FP rate for largest beads, the 390 μm beads (Table 4).

When demineralized water was replaced by sodium hyaluronate solution as a liquid phase, or when one third of the 390 μm beads was replaced by 156 μm beads, the FP rate decreased from 5 ± 1 to $0.7 \pm 0.6 \text{ N mm}^{-1}$ (Table 4), respectively, to $0.25 \pm 0.06 \text{ N mm}^{-1}$ (Table 5). This reduction was correlated with the decrease of the phase separation since the $L/(P+B)$ ratio of the extruded paste containing 1/3 of 156 μm beads and 2/3 of 390 μm beads (for a total of 42 wt.% of beads) dropped to $21.2 \pm 0.1 \text{ wt.}\%$, which corresponded to the $L/(P+B)$ ratio of the initial paste.

3.4. Size separation

Whatever the size and the proportion of included beads, the P/B ratio of the paste extruded during the first 40 mm of plunger displacement was significantly lower than the initial value (Figs. 7 and 8). Also, the P/B ratio increased slowly along the plunger displacement. In other words, beads were initially extruded preferentially compared to β -TCP powder, which resulted in the enrichment in powder (higher P/B value) of the paste remaining in the syringe (Figs. 7 and 8). This evolution was observed for all but one tested pastes. The exception was for the highest tested amount (42 wt.%) of the biggest beads (390 μm) for which an increase of P/B ratio was observed (Fig. 8). As a consequence, the paste remaining in the syringe was powder-depleted and its P/B ratio was only $82 \pm 13 \text{ wt.}\%$. Interestingly, when the paste was also prepared with 42 wt.% of the same sized beads, but using the sodium hyaluronate solution instead of water as a liquid phase, the evolution of the P/B ratio followed the same trend as previously

Table 6
 $L/(P+B)$ ratio of extruded paste (from 0 to end) compared with $L/(P+B)$ ratio of the paste remaining in the syringe at the end of injection experiments.

Percentage of included beads (wt.%)	25% introduced $L/(P+B)$: $30.3 \pm 0.3\%$		42% introduced $L/(P+B)$: $22.1 \pm 0.1\%$	
	$L/(P+B)$ 0-end	$L/(P+B)$ syr	$L/(P+B)$ 0-end	$L/(P+B)$ syr
156 μm beads	$30.7 \pm 0.2\%$	$19 \pm 1\%$	$21.7 \pm 0.2\%$	$14 \pm 4\%$
203 μm beads	n.t.	n.t.	$20.6 \pm 0.1\%$	$14 \pm 2\%$
240 μm beads	n.t.	n.t.	$20.4 \pm 0.1\%$	$14.1 \pm 0.3\%$
390 μm beads	$30.2 \pm 0.4\%$	$20.5 \pm 0.4\%$	$35 \pm 3\%$	$13.9 \pm 0.1\%$

Results are displayed for different sizes and amounts of model beads ($n \geq 3$). Some mixtures were not tested (“n.t.”), so no values were reported.

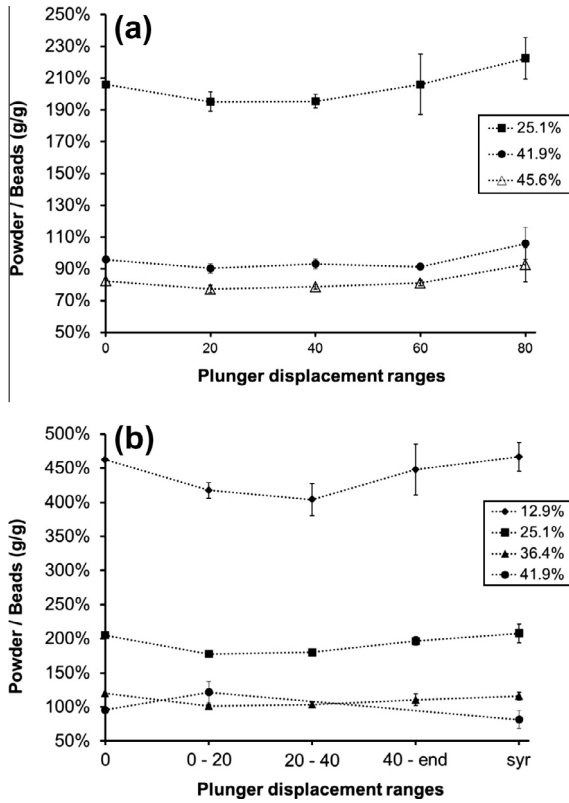


Fig. 7. (a) P/B ratio in extruded samples and in the remaining paste (“syr”) as a function of the plunger displacement range (0–20, 20–40 and 40–end) for different weight fractions of 156 μm beads. The bars represent the standard deviation. (b) P/B ratio in extruded samples and in the remaining paste (“syr”) as a function of the plunger displacement range (0–20, 20–40 and 40–end) for different weight fractions of 390 μm beads. The bars represent the standard deviation.

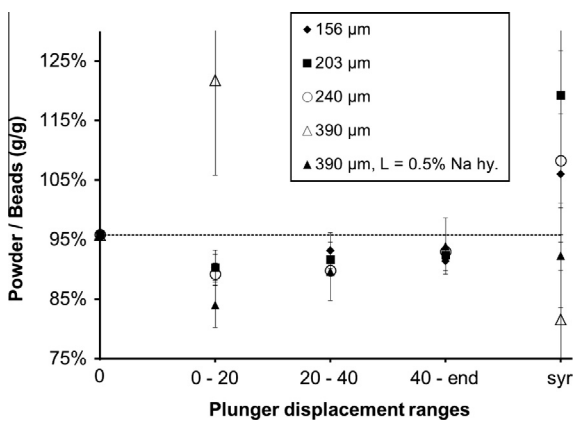


Fig. 8. P/B ratio in extruded samples and in the remaining paste (“syr”) as a function of the plunger displacement range (0–20, 20–40 and 40–end) for different bead sizes. All pastes included the same weight ratio of beads equal to 42 wt.%. Except for the symbols (▲) (L = 0.5% Na hyaluronate solution), the liquid phase was demineralized water. The bars represent the standard deviation.

described for lower bead contents: the extruded P/B ratio was low during the first millimeters and kept increasing during the injection test (Fig. 8).

These results show that larger particles (beads) moved with a different speed than the smaller ones (powder) and raised the question whether bead size separation occurred during injection. To answer this question, the size distribution of the beads collected from the different fractions of extruded pastes (“0–20”, “20–40”,

“40–end” and “syr”) was measured. An example of the cumulative size distributions that were obtained with a paste containing 25 wt.% of 156 μm beads is presented in Fig. 9: the particle size distribution was gradually shifted towards smaller sizes all along the plunger progression. The median diameter D_{50} of each fraction of beads was calculated and statistical analysis was performed on the results. It highlighted that the D_{50} of the beads that were extruded during the first 20 mm of plunger displacement was always significantly higher than the D_{50} of the beads collected in the paste remaining in the syringe. This confirmed what was experienced with the separation between beads and powder: in all cases, larger particles tended to be extruded preferentially than smaller ones.

4. Discussion

The powder and beads used in this study were chosen to simulate the composition of pastes containing large and spherical particles into a solid phase generally composed of microparticles (~10 μm). To focus on the phase and size separation mechanisms occurring in such pastes, two choices were made. Firstly, the model pastes tested in this study did not set or harden. It is known from previous studies that the kinetics of setting reaction has an influence on the injectability of pastes [5,35]. However, the main aim here was not to report how much paste could be extruded but to examine the phenomena underlying phase and size separations. Secondly, to investigate the sole influence of the addition of beads, it was purposely chosen to incorporate non-soluble glass beads that would evolve neither during the injection process nor during the characterization stages (no solubilization, no degradation, no deformation, no absorption). This approach models the introduction of spherical particles which do not interact chemically with the carrier (hydrogel or cement paste) [29,31]. Importantly, both the glass beads and the β-TCP powder were hydrophilic and could be very easily mixed with the aqueous phase to form homogeneous pastes.

4.1. Characterization of powder and beads constituting the solid phase

The particle size distribution and the morphology of the β-TCP powder were similar to those of CaP powders commonly used for bone cements [8,31,35]. Moreover, the size ratio between the two components of the solid phase (P and B) varied between 44 and 156 (Table 2). Considering that the size of glass beads was also close to typical diameters of beads described in the literature

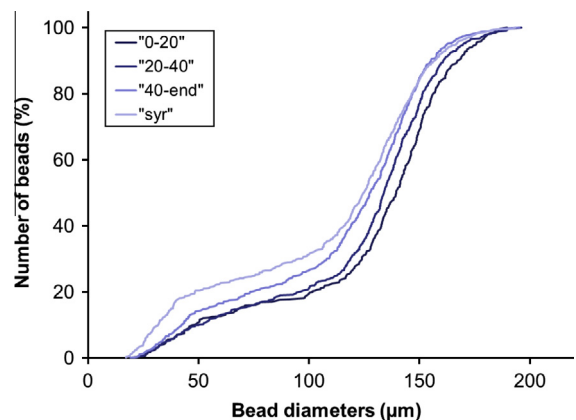


Fig. 9. Example of cumulative particle size distributions of the beads collected from the different samples of extruded paste corresponding to three different ranges of plunger displacement (0–20 mm, 20–40 mm, 40 mm to the injection halt) and of the paste which remained in the syringe at the end of the test. These results were obtained with one paste containing 25 wt.% of 156 μm beads.

[17,19,23,31], the size distributions and the size ratio of P and B were suitable to model real cement pastes at one point of their setting course.

In general, the D_{10} , the D_{50} and the D_{90} which were measured for the glass beads were smaller than those provided by the supplier (Table 2), presumably because the measurement method was different (image analysis vs. sieving).

4.2. Injectability and injection force

The profile of the injectability curves of pastes and putties was characteristic of mineral pastes extrusion, as described in previous studies [5,6,10,35]. The injectability curves could be decomposed in three distinct stages. The first stage, characterized by a transient and rapid increase of the load (Fig. 3b) was assigned to the compaction of the paste in the syringe [13]. This transient stage ended when the yield load required for the paste to start flowing through the syringe opening was reached [13,35]. This was always achieved before a 5 mm plunger course (Figs. 3 and 5), where the value for the injection load was measured.

In the second stage, the extrusion forces were characterized by a plateau in the absence of phase separation or by a slow increase when filter-pressing occurred [5,8,10,13]. Also, the scattering of the injection loads increased both with bead sizes and with volumes (Table 3, Figs. 3a and 5). The same observation was made for putties containing high contents of beads (>65 wt.%, data not shown). This could be related to an increase of bead–bead interactions.

In the last zone of the injection curves, loads increased sharply until the injection came to a halt (Figs. 3 and 5), either because all the paste had been extruded and the plunger met the end of the cannula or because, whatever the load, the paste remaining in the syringe at this point was no longer amendable to injection [6,33,35].

Even without any cannula, the reference paste (0% beads) was not completely injectable (injectability = $82 \pm 1\%$). This observation was consistent with results obtained by Habib et al.: although they worked with a higher displacement rate, which improves injectability [6], they needed a higher LPR (0.6 ml g^{-1}) to obtain a 100% injectable paste [33]. On the contrary, Montufar et al. obtained completely injectable pastes with the very same LPR (0.45 ml g^{-1}) and a lower displacement rate [35].

It is also worth noting that, in this study, the maximum injectability could never reach 100% since a small quantity of residual paste always remained in the tip of the syringe.

In the literature, the injectability of cement pastes was generally observed to decrease with an increase of particle size [5,8,15,35] and solid phase fraction [5–8,35]. This was correlated with an increase of injection force. The same behavior was observed with CaP beads injected in a hydrogel vehicle [29,31]. In the present case, increasing the size of included beads into pastes also led to a significant decrease of the injectability and to an increase of the injection load (Tables 3 and 4, Figs. 3 and 5). Increasing the fraction of 390 μm beads both in pastes and in putties had the same effect (Fig. 4), while for the 156 μm beads, a non-expected increase of the injectability was observed at moderate bead fraction (Table 3). This is very surprising and presently not understood.

In all cases, beyond a threshold value related to a certain volume of beads within pastes and putties, the injectability dropped abruptly (Fig. 4). It is assumed that, above this threshold, the beads formed a percolating network which completely blocked the motion of the plunger and prevented all further extrusion. The threshold value was markedly lower for larger beads, even though their bulk density was higher (Table 2). It is speculated that it is

related to the size ratio between the diameter of the syringe tip and the bead size.

Different routes have been proposed in the past to overcome the lack of injectability of mineral cement pastes [5,15,16]; two of them were selected based on the literature and investigated here. The first strategy was to increase the viscosity of the liquid phase [5,16]: substituting the demineralized water by a hydrogel (0.5% sodium hyaluronate solution) permitted to greatly improve the injectability of the pastes (from 35 ± 5 to $80 \pm 10\%$ for 42 wt.% of 390 μm beads, Fig. 4), as described in previous studies performed on usual cement pastes [5,16]. One explanation proposed in the past was that the sodium hyaluronate solution developed a thin lubricating layer between beads, hence decreasing the friction forces existing between powder particles, beads and syringe walls [5,29], and leading to lower injection forces. A different explanation was proposed recently based on the results of Habib et al. [36]. Indeed, since these authors observed that phase separation was continuous and started from the plunger side, they suggested that an increase of liquid viscosity decreased the propensity of the liquid to flow in between the solid particles to phase separate [36].

The second strategy to improve paste injectability was to use a broader bead size distribution, using a mixture of the smallest and the biggest beads (156 μm and 390 μm). This resulted in a large improvement of the injectability (Table 5), confirming what was observed in other studies for microparticles in usual CPC pastes [5,8,15]. The bimodal size distribution permitted the beads to be better packed (Table 5): the interparticle voids were reduced and the liquid migration hindered. It is also interesting to see that, contrarily to what was reported by Habib et al. when a small amount of fine CaP powder was added to a β -TCP–water paste [6], the injection load did not increase (Table 5).

4.3. Phase separation

Phase separation, also known as liquid migration, involves relative motions of liquids and solids within the syringe. It results in different displacement speeds between the liquid phase (L) and the solid phase (P + B) during injection processes. Thus, the determination of the L/(P + B) ratio of different portions of the pastes showed that phase separation was observed for all tested compositions, including the reference paste (0% beads) (Fig. 6). Considering the L/(P + B) ratios of the initial paste and of the paste after extrusion (Table 6, Fig. 6), and despite all the attention paid to minimize such experimental errors, there might have been an experimental bias (liquid evaporation or loss before weighting) which might be more pronounced for the paste remaining in the syringe than for the other fractions of paste. However, given the significant difference experienced between the L/(P + B) ratios of the extruded paste and of the paste remaining in the syringe, it can be concluded that all investigated pastes, without exception, were prone to phase separation. This observation was in agreement with another study devoted to the injection of β -TCP–water mixtures [6].

Interestingly, the addition of beads did not modify the overall paste behavior. The extruded L/(P + B) ratio was constant during the plunger displacement (from 0 to end, Fig. 6) and resulted in the drying of the paste remaining in the syringe (Table 6). Since the void space between solid particles (P + B) had to be filled with liquid to enable paste flow [37], once the paste was water-depleted and there was not enough liquid left, the injection stopped. At this point, the remaining paste was not injectable at all, whatever the applied load [6]. This would explain why the L/(P + B) ratio left in the syringe (“syr”) was constant for a given amount of beads (Table 6): the void volume which had to be filled with liquid for the paste to flow, i.e. the volume of the syringe which was not

occupied by the beads depended on their amount, and not on their sizes.

Investigating more thoroughly the injection curves also enabled us to gain insights into the phase separation mechanism. As discussed previously, these curves could be divided into three stages. The second region began when the paste first exited the syringe opening and stopped once the remaining paste was no longer injectable: it was therefore characteristic of the injection behavior of the paste. Especially, the slope of this part of the curve (i.e. the FP rate) could be used as a measure of the extent of phase separation between liquid and solid [10,13]: for example, including 42 wt.% of 390 μm bead within the paste, resulted in a strong phase separation since the extruded $L/(P+B)$ ratio was more than 1.5 times the initial one (Table 6). This was correlated to a high FP rate of $5 \pm 1 \text{ N mm}^{-1}$ (Table 3).

Such a high FP rate was not observed with smaller beads: the amount of introduced beads played a significant role in phase separation only for the largest beads; this could indicate that in the investigated conditions, 390 μm (less than five times smaller than the diameter of the syringe opening) was close to the maximum size allowing injection. Thus, the introduction of such large beads in both pastes and putties highlighted phenomena which were not observed for smaller bead sizes.

When the pressure required to filter the liquid through the particles was lower than the extrusion pressure of the paste, filter-pressing occurred [28,31,37]. In other words, improving the packing of the particles or increasing the liquid phase viscosity both permitted the decrease in liquid migration. As demonstrated by the increase of the bulk densities (Table 5), the beads were better packed when blending 156 μm beads with 390 μm beads instead of using only beads of one size. This resulted, for pastes containing 1/3 of 156 μm beads and 2/3 of 390 μm beads, in an extruded $L/(P+B)$ ratio equal to the $L/(P+B)$ ratio of the initial paste. Once again, the drastic reduction of the FP rates (Tables 4 and 5) correlated very well with the decrease of the filter-pressing phenomenon.

4.4. Size separation

It has been shown that phase separation between liquid and solid phases occurred in the pastes during the injection tests. Since it is known that in multimodal suspensions, fine particles behave as a fluid toward coarser particles, especially if the size ratio between larger and smaller particles is 10 or more [32], the question arose whether size separation occurred between coarser glass beads (100–500 μm) and smaller β -TCP particles (1–10 μm) [33]. To investigate this point, the evolution of the β -TCP powder-to-beads ratio (P/B , w/w) was plotted with respect to plunger displacement (Figs. 7 and 8).

The extruded P/B ratio was low during the first millimeters and increased along with the displacement of the plunger, showing that beads were extruded preferentially when compared to β -TCP powder. This result was quite surprising since the opposite was expected [32]. This might arise from the formation of a dense cake of powder particles at the rear of the syringe, behind the beads. Thus, all along the plunger displacement, the filter cake would progress and push the beads forward. This is shown by the significant increase of the P/B ratio throughout the injection process (Figs. 7 and 8). Interestingly, the overall behavior of the paste was not changed when water was replaced by a hydrogel (Fig. 8). In fact, there was size separation not only between powder and beads but also within beads, as shown by the evolution of the bead size distribution during injection (Fig. 9).

Only in the pastes containing 42 wt.% of 390 μm beads and prepared with water as a liquid phase, the extruded P/B ratio was higher than that of the initial paste (Fig. 8). But in this case, the

paste was poorly injectable (only $35 \pm 5 \text{ wt.}\%$ was extruded) and the injection process stopped very rapidly, before size separation occurred (Table 4, Fig. 3a). In other words, it is speculated that size separation occurs more slowly than phase separation.

To our knowledge, this is the first study where size separation of the components of a mineral paste has been demonstrated during injection tests. Habib et al. [33] first raised this question but could not show any significant variation of the size (D_{10} , D_{50} and D_{90}) of the solid phase particles during the injection process. They concluded that, in their case, there was no occurrence of size separation. However, their pastes were composed of a mixture of water and β -TCP powder with a size in the micrometer range. Also, the particle size distribution was fairly narrow.

5. Conclusions

The present results showed that the injectability of pastes and putties loaded with millimeter-sized glass beads decreased with increasing size and amount of beads. This was directly related to the phase separation between liquid, which was extruded preferentially, and the solid phase. This filter-pressing phenomenon was highlighted thanks to the monitoring of the composition of the extruded paste. It was also shown that a high filter-pressing rate (slope of the injection curve in the intermediate range) correlated very well with the occurrence of liquid migration and that it could be used as an indicative parameter. For example, for 42 wt.% of 390 μm beads inside the paste, the FP rate rose to 5 N mm^{-1} and the ratio of liquid to solid phase in the extruded paste was nearly three times as high as in the paste remaining in the syringe. When the volume occupied by the beads was increased above a threshold value, the injection process was prematurely stopped: the injectability of pastes and putties sank abruptly. This threshold value decreased with increasing bead diameter: it was below 42 wt.% of beads within the pastes when 390 μm beads were used and above 45 wt.% with 156 μm beads. This threshold value also depended on the liquid phase used to prepare the pastes. Indeed, using a hydrogel solution instead of demineralized water did not change the overall paste behavior, but it increased the threshold value and increased the amount of extruded paste.

This study also revealed that two separation mechanisms occurred simultaneously during injection: not only the liquid but also the beads moved faster than the β -TCP powder particles or, in other words: injection mobility (L) > mobility (B) > mobility (P). This led to the formation of a dense powder cake at the rear of the syringe. The present results suggest that phase separation occurs faster than size separation.

Interestingly, mechanisms and phenomena related to poor injectability were shown to be similar in pastes with and without hydrogel, and in putties. Therefore, their understanding is of interest for the formulation of optimized injectable formulations. This is especially true since it was shown that phase and size separations were amplified by the use of milli-sized particles, which is a growing trend in the field of injectable biomaterials.

Acknowledgements

The authors wish to thank S. Grünenfelder, G. Bigolin, C. Wälti and S. Honold for their technical help in this study.

Appendix A. Figures with essential colour discrimination

Certain figures in this article, particularly Figures 1, 3, 5 and 9, are difficult to interpret in black and white. The full colour images can be found in the on-line version, at <http://dx.doi.org/10.1016/j.actbio.2013.12.018>.

References

- [1] Brown WE, Chow LC. A new calcium phosphate setting cement. *J Dental Res* 1983;62:672.
- [2] LeGeros RZ, Chohayeb A, Shulman A. Apatitic calcium phosphates: possible dental restorative materials. *J Dental Res* 1982;61:343.
- [3] Dorozhkin SV. Calcium orthophosphate cements and concretes. *Materials* 2009;2:221–91.
- [4] Ginebra MP, Espanol M, Montufar EB, Perez RA, Mestres G. New processing approaches in calcium phosphate cements and their applications in regenerative medicine. *Acta Biomater* 2010;6:2863–73.
- [5] Bohner M, Baroud G. Injectability of calcium phosphate pastes. *Biomaterials* 2005;26:1553–63.
- [6] Habib M, Baroud G, Gitzhofer F, Bohner M. Mechanisms underlying the limited injectability of hydraulic calcium phosphate paste. *Acta Biomater* 2008;4:1465–71.
- [7] Khairoun I, Boltong MG, Driessens FCM, Planell JA. Some factors controlling the injectability of calcium phosphate bone cements. *J Mater Sci Mater Med* 1998;9:425–8.
- [8] Tadier S, Bolay NL, Fullana SG, Cazalbou S, Charvillat C, Labarrère M, et al. Cogrounding significance for calcium carbonate–calcium phosphate mixed cement. II. Effect on cement properties. *J Biomed Mater Res B Appl Biomater* 2011;99 B:302–12.
- [9] Bayfield M, Haggett JA, Williamson MJ, Wilson DI, Zargar A. Liquid phase migration in the extrusion of icing sugar pastes. *Trans IChemE* 1998;76C:39–46.
- [10] Davies J, Binner JGP. Plastic forming of alumina from coagulated suspensions. *J Eur Ceram Soc* 2000;20:1569–77.
- [11] Lin CY, Kellett BJ. General observations of constant flow rate filter pressing. *J Am Ceram Soc* 1998;81:2093–108.
- [12] Patel MJ, Blackburn S, Wilson DI. Modelling of paste flows subject to liquid phase migration. *Int J Numer Meth Eng* 2007;72:1157–80.
- [13] Rough SL, Wilson DI, Bridgwater J. A model describing liquid phase migration within an extruding microcrystalline cellulose paste. *Trans IChemE* 2002;80A:701–14.
- [14] Yu AB, Bridgwater J, Burbidge AS, Saracevic Z. Liquid maldistribution in particular phase extrusion. *Powder Tech* 1999;103:103–9.
- [15] Gbureck U, Spatz K, Thull R, Barralet JE. Rheological enhancement of mechanically activated alpha-tricalcium phosphate cements. *J Biomed Mater Res B Appl Biomater* 2005;73:1–6.
- [16] Leroux L, Hatim Z, Freche M, Lacout JL. Effects of various adjuvants (lactic acid, glycerol, and chitosan) on the injectability of a calcium phosphate cement. *Bone* 1999;25:315–45.
- [17] Chen W, Zhou H, Weir MD, Bao C, Xu HHK. Umbilical cord stem cells released from alginate-fibrin microbeads inside macroporous and biofunctionalized calcium phosphate cement for bone regeneration. *Acta Biomater* 2012;8:2297–306.
- [18] Félix Lanao RP, Leeuwenburgh SCG, Wolke JGC, Jansen JA. Bone response to fast-degrading, injectable calcium phosphate cements containing PLGA microparticles. *Biomaterials* 2011;32:8839–47.
- [19] Fullana SG, Ternet H, Freche M, Lacout JL, Rodriguez F. Controlled release properties and final macroporosity of a pectin microspheres–calcium phosphate composite bone cement. *Acta Biomater* 2010;6:2294–300.
- [20] Habraken WJEM, Wolke JGC, Jansen JA. Ceramic composites as matrices and scaffolds for drug delivery in tissue engineering. *Adv Drug Delivery Rev* 2007;59:234–48.
- [21] Habraken WJEM, Zhang Z, Wolke JGC, Grijpma DW, Mikos AG, Feijen J, et al. Introduction of enzymatically degradable poly(trimethylene carbonate) microspheres into an injectable calcium phosphate cement. *Biomaterials* 2008;29:2464–76.
- [22] looss P, Le Ray AM, Grimandi G, Daculsi G, Merle C. A new injectable bone substitute combining poly(ϵ -caprolactone) microparticles with biphasic calcium phosphate granules. *Biomaterials* 2001;22:2785–94.
- [23] Qi X, Ye J, Wang Y. Improved injectability and in vitro degradation of a calcium phosphate cement containing poly(lactide-co-glycolide) microspheres. *Acta Biomater* 2008;4:1837–45.
- [24] Schnieders J, Gbureck U, Thull R, Kissel T. Controlled release of gentamicin from calcium phosphate-poly(lactic acid-co-glycolic acid) composite bone cement. *Biomaterials* 2006;27:4239–49.
- [25] Takagi S, Chow LC. Formation of macropores in calcium phosphate cement implants. *J Mater Sci Mater Med* 2001;12:135–9.
- [26] Xue Z, Zhang H, Jin A, Ye J, Ren L, Ao J, et al. Correlation between degradation and compressive strength of an injectable macroporous calcium phosphate cement. *J Alloys Compounds* 2012;520:220–5.
- [27] Apelt D, Theiss F, El-Warrak AO, Zlinszky K, Bettschart-Wolfsberger R, Bohner M, et al. In vivo behavior of three different injectable hydraulic calcium phosphate cements. *Biomaterials* 2004;25:1439–51.
- [28] Bohner M, Tadier S, van Garderen N, de Gasparo A, Doebelin N, Baroud G. Spherical calcium phosphate particles for dental and orthopaedic applications: synthesis and applications. *Biomater* 2013;3:e25103.
- [29] Fatimi A, Tassin J-F, Bosco J, Deterre R, Axelos MAV, Weiss P. Injection of calcium phosphate pastes: prediction of injection force and comparison with experiments. *J Mater Sci Mater Med* 2012;23:1593–603.
- [30] Gauthier O, Khairoun I, Bosco J, Obadia L, Bourges X, Rau C, et al. Noninvasive bone replacement with a new injectable calcium phosphate biomaterial. *J Biomed Mater Res* 2003;66A:47–54.
- [31] Oliveira SM, Barrias CC, Almeida IF, Costa PC, Pena Ferreira MR, Bahia MF, et al. Injectability of a bone filler system based on hydroxyapatite microspheres and a vehicle with in situ gel-forming ability. *J Biomed Mater Res B Appl Biomater* 2008;87:49–58.
- [32] Farris RJ. Prediction of the viscosity of multimodal suspensions from unimodal viscosity data. *Trans Soc Rheol* 1968;12:281–301.
- [33] Habib M, Baroud G, Gitzhofer F, Bohner M. Mechanisms underlying the limited injectability of hydraulic calcium phosphate paste. Part II. Particle separation study. *Acta Biomater* 2010;6:250–6.
- [34] Tadier S, Galea L, Gruenenfelder S, Bohner M. Investigation of the phase separation occurring during the injection of β -tricalcium phosphate–water–glass beads pastes. *Key Eng Mater* 2012;493–494:693–7.
- [35] Montufar EB, Maazouz Y, Ginebra MP. Relevance of the setting reaction to the injectability of tricalcium phosphate pastes. *Acta Biomater* 2013;9:6188–98.
- [36] Habib M, Baroud G, Galea L, Bohner M. Evaluation of the ultrasonication process for injectability of hydraulic calcium phosphate pastes. *Acta Biomater* 2012;8:1164–8.
- [37] Blackburn S, Böhm H. Influence of powder packing on paste extrusion behaviour. *Trans IChemE* 1993;71A:250–6.